Journal of Materials Chemistry C

Accepted Manuscript

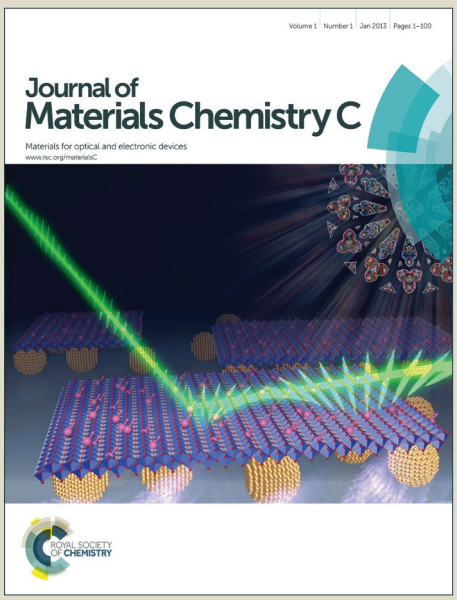

ROYAL SOCIETY OF CHEMISTRY

www.rsc.org/materialsC

Preparation by RF-sputtering and p-type conducting transparent characteristics of delafossite Mg-doped $CuCrO_2$ thin films.

A. Barnabé*, Y. Thimont, M. Lalanne, L. Presmanes, P. Tailhades.

Université de Toulouse, Institut Carnot CIRIMAT – UMR CNRS-UPS-INP 5085,

Université Paul Sabatier, 118 route de Narbonne, 31062 Toulouse Cedex 9, France.

* Corresponding Author: barnabe@chimie.ups-tlse.fr

KEYWORDS: p-type TCO, thin film, delafossite, rf-sputtering, electronic properties, optical modelling.

ABSTRACT: The growth of technologically relevant compound Mg-doped $CuCrO_2$ delafossite thin films on quartz substrate by radio-frequency sputtering is reported in this work. The deposition, performed at room temperature leads to nanocrystallized phase with extremely low roughness and high density. Delafossite characteristic diffraction peaks were obtained as a function of the thermal treatment under a primary vacuum. The electrical conductivity was optimized until 1.6 S/cm with an optical transmittance of 63 % in the visible range by a 600 °C annealing treatment under primary vacuum applied for 4 h. The transport properties were analyzed by Seebeck, Hall measurement, integrated spectrophotometry and optical simulation. These measurements highlighted degenerated semiconductor behavior with hopping mechanism with high holes concentration (10^{21} cm^{-3}) and low mobility (0.2 $cm^2V^{-1}s^{-1}$). The direct optical bandgap of 3.3 eV has been measured according to the Tauc's relation. A refractive index of 2.3 at a wavelength of 1100 nm has been determined by spectroscopic ellipsometry and confirmed by two independent modellings of the optical transmittance and reflectance spectra. All these p-type TCO optoelectronic characteristics lead to the highest Haacke's Figure Of Merit (1.5×10^{-7} Ω^{-1}) reported so far for such delafossite materials.

1. Introduction

Metal oxides are a class of materials showing one of the greatest range of properties and are more and more attractive for various applications. Metal-oxygen bond is strong so that the oxides have a combination of a high heat of formation and a wide band gap. Of particular interest are the wide-bandgap oxide semiconductors also called Transparent Conducting Oxides (TCO) which combine electrical conductivity and optical transparency in a single material (1)(2). Therefore, TCO thin films are used as transparent electrodes in numerous technological applications including photovoltaic cells, flat panel displays, electromagnetic shielding devices, transparent heat sources and light emitting diodes (3). The majority and most popular TCO currently available are n-type electron conductors. P-type TCO has only been reported in 1997 for copper-based delafossite material $CuAlO_2$ (4). Since then, a number of promising wide bandgap p-type hole conductors materials have been found as a consequence of material exploration efforts following the design concept (5-9). Many works over the last few years has led to the description of a number of p-type TCO based on copper-based delafossite $CuMO_2$ oxides with M = Ga (10-11), In (12), Y (13), Sc (14) for instance. Among them, $CuCrO_2$ based film prepared by radio frequency sputtering reaches a conductivity of 220 $S.cm^{-1}$, which is the highest conductivity in p-type TCO but in return with a limited optical transmittance in the visible region (15).

In addition, some delafossite based $CuMO_2$ films have been used for application in transparent diode and UV-emitting diode devices (10) with various n-type TCO counterparts. Realization of such p-/n- transparent hetero-junction makes it possible to investigate the possibility of invisible circuits based on transparent oxides (16; 17), which are not feasible with n-type materials alone.

To achieve this aim from an application stand point, a lot of difficulties have to be solved. First, it is necessary to be able to deposit the resulting material as a thin film on a transparent substrate. This has been already published with different deposition techniques and with a large range of deposition conditions. However, the main TCO performance of these p-type thin film materials still needs improvements to, in fine, reach those of their n-type TCO counterparts. Second, proper control of the substrate temperature over the entire process sequence is required and may become an important issue for realistic applications since conventional or flexible substrates are required. For the $CuMO_2$ thin film, only very few data concerning the development of this class of material at low temperature, i.e. below 450 °C, have been published among all the references (18). This is explained by the fact that the development of this phase requires high temperatures and strict conditions of preparation to be pure. The use of

high temperatures needed for the successful crystallization of delafossite phases requires the use of heat-resistant substrates, which are relatively expensive. In addition, stabilization of monovalent noble metal cation A(I) in delafossite A(I)M(III)O_2 is not always possible in such conditions due to the natural tendency of this cation to decompose before forming reaction appears.

Among $CuMO_2$ systems with various M-cation and appropriate dopants, magnesium-doped $CuCrO_2$ films present conductivity greater than many other p-type TCO, suitable band gap and quite low temperature processing. Hence, Mg-doped $CuCrO_2$ films is considered as one of the most potential candidate for opto-electronic applications (15, 19). On top of that, $CuCrO_2$ based material has also been studied for its antibacterial (20), catalytic and photo-catalytic (21-24), magnetic (25-27), thermoelectric (28-32), multiferroic and magneto-electric (33; 34) properties, sensors (35) photovoltaic cells (36) and batteries (37).

The synthesis and complete optical and electrical characterizations of Mg-doped $CuCrO_2$ delafossite thin film using a radio-frequency sputtering technique is reported in this paper. In addition with previous work done on $CuFeO_2$ (18) it contributes to a better understanding of the complex reactions involved during the delafossite phase formation, in order to develop a versatile method for preparing thin films of oxide structure on copper-based delafossite $CuMO_2$ at relatively low temperature.

2. Materials and methods

Preparation of Mg-doped $CuCrO_2$ sputtering target material: Due to the very limited Mg^{2+} solubility range in the delafossite $CuCrO_2$ structure and then to prevent the precipitation of a secondary spinel phase which can affect the physical properties (26; 38; 39), the Mg content in Mg-doped $CuCrO_2$ was fixed to 3%$^{at.}$ in this study. Polycrystalline $CuCr_{0.97}Mg_{0.03}O_2$ powder (noted Mg-doped $CuCrO_2$ in the manuscript) was prepared by grinding and mixing the starting commercial oxides Cu_2O, Cr_2O_3 and MgO. The stoichiometric oxide mixture was treated at 900 °C for 10 h in an ambient nitrogen atmosphere and cooled down to room temperature. After it was reground, the mixture was refired for a further 10 h period. X-Ray Diffraction (XRD) measurements performed with a Bruker D4 Endeavor X-ray diffractometer (copper radiation $\lambda CuK_{\alpha 1}$ = 1.5405 Å and $\lambda CuK_{\alpha 2}$ = 1.5445 Å) showed a rhombohedral $R\bar{3}m$ delafossite phase with traces of magnesiochromite (Figure 1) in good agreement with the very limited Mg^{2+} solubility range in $CuCr_{1-x}Mg_xO_2$ (26).

The lattice parameters determined by the Rietveld method implemented in the Fullprof/WinPlotR program are a = 2.9755(2) Å and c = 17.091(3) Å. In comparison with the undoped $CuCrO_2$ phase elaborated in the same experimental condition whereas a = 2.9742(2) Å and c = 17.090(3) Å (40), a slight increase of the lattice parameter could be observed. This supports the partial integration of the magnesium specie on the octahedral-site of the delafossite structure as it well agrees the increase of the average ionic radius as chromium with $r(Cr^{3+}_{Coord.VI})$ = 0.615 Å is replaced by magnesium with $r(Mg^{2+}_{Coord.VI})$ = 0.720 Å.

The polycrystalline delafossite powder was then pressed into 10 cm in diameter sputtering target and sintered at 1200 °C for 10 h in air. The relative density of the target was about 60 %. XRD measurement carried out on a small representative pellet showed no foreign phases.

Preparation of Mg-doped $CuCrO_2$ thin film material: To produce desired thin films, the target assembly was attached to an Alcatel A450 Radio Frequency (RF) magnetron sputtering chamber. Prior to the film deposition, pre-sputtering by argon plasma for 10 min was performed to remove surface contamination. Pre-cleaned fused quartz microscope substrates (25 × 25 mm, ≈ 1 mm thick from Electron Microscopy Sciences Ref #72250-01) placed on a water-cooled sample holder, were used. The deposition parameters summarized in Table 1, were optimized in terms of RF-power, magnetron, internal gas pressure and target to substrate distance, in order to keep constant the nominal oxygen stoichiometry of the target thanks to previous work on $CuFeO_2$ thin film materials (18; 41). In this condition the average deposition rate deduced from thickness measurements done by both surface profilometry and X-ray reflectometry, was equal to 8.5 nm/min. Films with thicknesses in the range of 50 to 300 nm were deposited. Effective Mg-doping of the films was confirmed by electron probe micro-analysis (EPMA) using a Cameca SX 50 apparatus. From a minimum of ten measurements performed on films deposited on silicon substrate, 0.7-0.8 atomic percent was obtained for the Mg content over the whole species (Cu+Cr+Mg+O). Expressed over the (Cr+Mg) content, it corresponds to an overall Mg-doping level of 3 atomic percent identical to the target composition.

The as-deposited films deposited on quartz substrates have been annealed for 4 h under primary vacuum at various temperatures ranging from 450 to 800 °C, to obtain the delafossite Mg-doped $CuCrO_2$ material.

Characterization: The structural properties of the films were investigated on 300 nm thick films by α = 1° Grazing Incidence XRD (GIXRD) at room temperature and Temperature dependent XRD (TXRD). GIXRD was performed with a Siemens D5000 diffractometer equipped with a Bruker Sol-X detector. TXRD was performed with a Bruker D8 diffractometer in Bragg-Brentano θ-θ geometry equipped with a Bruker LynxEye 1D detector and an Anton Paar HTK1200N temperature chamber. In all cases, copper radiations were used as the X-ray source ($\lambda CuK_{\alpha 1}$ = 1.5405 Å and $\lambda CuK_{\alpha 2}$ = 1.5445 Å).

The microstructure of the films was observed by a Jeol JSM-6400 field emission gun Scanning Electron Microscope (SEM) and Nanoscope III Dimension 3000 Atomic Force Microscope (AFM). SEM and AFM surface views were analyzed using the Gwyddion software (42).

The electrical resistivity was measured using a Signatone four-point probe measurements unit. A Versalab Quantum Design Physical Properties Measurement System (PPMS) with an applied external field of 3 T was used for the Hall measurements. A

home-made room temperature Seebeck measurement device with gold probe contacts and adapted to the thin film geometry was used for thermoelectric characterizations.

The optical characteristic of the thin films were investigated in the 300 to 1100 nm wavelength range with a Bentham PVE300 UV/Visible/IR integrated spectrophotometer, then the spectra were modeled using the SCOUT software (43). The ellipsometry technique has been used for the determination of the optical index. Measurements were carried out with a Jobin-Yvon/Horiba Uvisel spectroscopic ellipsometer (SE), in the 350 to 1000 nm spectral range. Ellipsometry data were recorded at an incidence angle of 70 deg. and were analyzed using the Delta-Psi 2 software (shell version 2.9). A sample stack structure (quartz / film / surface layer) was employed to extract the optical constants (n and k) of thin films.

3. Results and discussion

Structural analysis: The as-deposited thin film is amorphous according to XRD measurement (Figure 2a). For this sample, no dominant diffraction peak could be observed because of the nanocrystalline nature of films as previously observed in such similar systems with Cr (15; 44) and Fe (18).

Heat treatments have then been carried out up to 800 °C in order to highlight the phases which could be crystallized or formed. The TXRD patterns recorded in Bragg-Brentano geometry in the 450 to 800 °C temperature range are displayed in Figure 2a. Such treatments were carried out under primary vacuum to avoid oxidation of the pristine phase. Actually, a thermal treatment under air atmosphere above 450 °C (TXRD done in this work but not shown here) leads to the formation of spinel $CuCr_2O_4$ with concomitant appearance of tenorite CuO in good agreement with previous reports (45).

From the TXRD diffractograms and for T > 500 °C, a main broad and secondary diffraction peaks can be identified at 2θ ≈ 36 ° and ≈ 62 °, i.e. with d_{hkl} ≈ 2.5 Å and ≈ 1.5 Å respectively. It is difficult to match one particular phase among $CuCrO_2$, Cu_2O, and Cr_2O_3 to these TXRD patterns due to the overlap of the main diffraction peaks, the geometry and temperature chamber contributions and thermal expansion. However, the splitting of the broad main peak located at around 36 ° into two peaks at higher and lower 2θ value with a concomitant increase and decrease of their intensities respectively, is in good agreement with the *(012)* and *(101)* Bragg reflexions of the Mg-doped $CuCrO_2$ phase. The secondary peak located at 2θ ≈ 62 ° also belongs to the delafossite-type structure with the *(110)* reflexion.

From α = 1° GIXRD measurements carried out at room temperature on annealed samples in the same temperature range (Figure 2b), the *(012)* and *(110)* peaks could be more finely located at 36.5 and 62.7 ° in the 2θ range. Additional characteristic peaks belonging to the delafossite-type Mg-doped $CuCrO_2$ are also highlighted at 2θ ≈ 31.5, 41.0, 71.9 and 74.9 ° and correspond to the *(006)*, *(104)*, *(116)* and *(202)* Bragg peaks respectively.

All the XRD results consequently suggested that the samples annealed above 500 °C were composed of delafossite-type Mg-doped $CuCrO_2$. The lattice parameters a = 2.959(3) Å, c = 17.06(9) Å and V = 129.36 $Å^3$ of the $CuCrO_2$ thin film determined from GIXRD pattern matching refinement on sample annealed at 750 °C are in good agreement with bulk Mg-doped $CuCrO_2$ data.

Despite the high anisotropic character of the delafossite structure and contrary to previous studies whereas normal or highly c-axis polycrystalline delafossite films were obtained by various methods and/or conditions (sol-gel (45-47), chemical solution deposition (48), pulsed laser deposition (49)), this structural characterization indicates that the *(00l)* reflexion of the delafossite structure is always very weak. This result was already reported in the literature for such $CuCrO_2$ films (15; 44; 50-51) and could be correlated to the oxygen stoichiometry of the growing phases.

In this work, the use of non-reactive magnetron RF sputtering of Mg-doped $CuCrO_2$ target yields in limited and controlled oxygen loss during the deposition process and finally assists in the formation of the delafossite phase without *(00l)* preferred orientation (52) in the limit of the reduction of Cu(I) species into metallic copper nanoparticles (41; 53). The expected stoichiometric oxygen content was independently supported by EPMA measurements carried out on silicon substrates whereas the cation (Cu+Cr+Mg) to anion (O) atomic ratio was found to be equal to 1 in the limit of the accuracy of the technique.

Microstructural analysis: The SEM image of the 300 nm as-deposited film in cross-section view (Figure 3a) reveals dense thin film with very small particle size. An extremely low Root Mean Square (RMS) roughness estimated to RMS = 0.4 nm is determined by AFM (Figure 3b). This very weak surface topography is in good agreement with previous studies on delafossite materials deposited within the same (non-reactive magnetron sputtering of oxide target) (18) or similar (reactive magnetron sputtering of metallic target) (54) deposition condition. It also explains the impossibility to obtain exploitable SEM planar view even by the use of field emission gun source. One can note that for a lower thickness of 100 nm, the as deposited film still presents a smooth surface with very low roughness (RMS close to 0.8 nm) and small grain size (Figure 3c and Figure 3d).

The AFM analysis of the Mg-doped $CuCrO_2$ thin films annealed at different temperature reveals an important influence of the annealing temperature on the microstructure due to promotion of atom diffusion. For a film thickness of 100 nm, the Figure 4 shows the topographies obtained for the different annealing temperatures in between 450 and 700 °C.

In comparison with the pristine phase (100 nm as-deposited thin film shown in Figure 3c and Figure 3d), the 450 °C annealed thin film exhibits well-defined grain shape with an average grain size of around 50 nm. From 450 to 600 °C, a constant decrease of the average grain size D and root mean square RMS clearly indicate crystallization and densification processes in perfect agree-

ment with the XRD analysis. At 600 °C which corresponds to the minimum temperature evidenced by TXRD analysis to obtain a characteristic splitting of the broad main diffraction peak into the *(012)* and *(101)* Bragg reflexions of the Mg-doped $CuCrO_2$ phase, AFM shows a smooth surface with a minimum RMS value. Above 600 °C, small grains re-appear.

Even if the very weak surface roughness obtained for the as-deposited film is largely observed in many studies, the specific deposition conditions used in this work allows highlighting a particular microstructural evolution versus annealing temperature. Indeed, the normal growth of the crystallites with temperature is followed by a reverse phenomenon leading to a decrease of this size and the decay of the roughness, at about 600 °C. To a lesser extent, this behavior was also observable in thin films deposited by reactive RF magnetron sputtering by R.S. Yu et al. (54).

Four probes measurement: The transport properties of 100 nm and 300 nm thick as-deposited and annealed films were determined by in line four probes measurement at room temperature. The temperature dependence of the electrical conductivity σ for each compound is shown in Figure 5a. The thickness dependence of electrical properties expressed in sheet resistance ($R_{\square}$) is also plotted in Figure 5b for film annealed at various temperatures.

Whatever the thickness, the as-deposited Mg-doped $CuCrO_2$ thin films show an electrical conductivity σ lower than 0.0045 $S.cm^{-1}$. This electrical conductivity increases with the annealing temperature especially from 450 °C and reaches its maximum value σ = 1.4 $S.cm^{-1}$ at 600 °C. For higher temperature, σ tends to decrease. For these temperatures, no increase in conductivity with the annealing time has been noticed. The optimal annealing temperature (T = 600 °C) corresponds to the particular changes in the structural and microstructural behaviors: it's high enough to crystallize the delafossite phase but not too low to generate grain boundary resistivity. This result is consistent with the literature whereas some conductivities are reported for various annealing and/or deposition temperatures, for various deposition techniques and for various Mg-doping level (RF-sputtered $CuCrO_2$ at T (15), $CuCrO_2$ sol-gel processed and post-annealed at T (45), chemical solution deposited $CuCr_{0.95}Mg_{0.05}O_2$ and post-annealed at T (48), pulsed laser deposited $CuCr_{0.92}Mg_{0.08}O_2$ at T (55) and pulsed laser deposited $CuCr_{0.92}Mg_{0.08}O_2$ at T (56)). For comparison, values issued from these works are reported in Figure 5a.

The transport measurement proceeded as a function of the temperature under air atmosphere, permits to determine the transport activation energy of all the annealed thin films. The transport activation energy decreases progressively until a stabilized value of 0.055 eV after a 600 °C annealing process. The stabilized value has also been reported by Rastogi et al. (57). The activation energy is less than 3kT and justifies an important number of acceptor levels near the top of the valence band. This behavior corresponds to a highly doped degenerated semiconductor behavior. We noticed that this transport activation energy could increase from 55 meV at 250 °C to 63 meV at 450 °C under air then returns to 55 meV when the temperature drops to room temperature. This cycle generates also a permanent impact on the electrical conductivity which increases from 0.96 $S.cm^{-1}$ to 1.07 $S.cm^{-1}$ after the under air thermal cycle process. This behavior was explained by the intercalation of oxygen atoms in the copper plan of the delafossite structure according to the $(Cu^{+}_{1-x-2\delta}Cu^{2+}_{x+\delta})(Fe^{3+}_{1-x}Mg^{2+}_{x})O_{2+\delta}$ formulae.

The electrical conductivity versus temperature in between 150 and 400 K cannot be completely fitted by a classical thermal power law (adapted for classical semiconductors) in particular to the lower temperatures. Nevertheless, the σ(T) curves can be fitted by the following two dimensions Mott relation (Equation 1):

$$\sigma(T) = A \cdot \exp\left(-\frac{T_{Mott}}{T}\right)^{1/n} \quad \text{(Equation 1)}$$

where σ is the material conductivity, A is an exponential pre-factor, T_{Mott} the Mott temperature and n = 3 corresponds to the two dimensions transport. The σ(T) behavior is in agreement with the hopping carrier mechanism.

Hall measurement: DC Hall measurements were processed on a 300 nm film annealed at 600 °C for 4 h under vacuum and previously connected on PPMS support by 20 µm aluminum wires thank to Van der Pauw geometry. 3 T magnetic field and 0.05 mA current were applied to measure the electric potential. Nevertheless, no Hall effect has been measured by this DC technique with a moderate applied magnetic field. This supposes a too small carriers mobility and/or a too high carrier concentration which make sense with a hole concentration of about 10^{21} cm^{-3} reported by O'Sullivan et al. (34) on similar materials ($CuCr_{0.90}Mg_{0.10}O_2$) with AC Hall measurement using a magnetic field of 14 T.

Seebeck measurement: Figure 6 shows the annealing temperature dependence of the Seebeck coefficient (S) measured at room temperature for the 100 nm thick Mg-doped $CuCrO_2$ films (300 nm thick films exhibit identical values and are not shown on this graph but are listed in Table 2). Whatever the thicknesses and the annealing temperatures (including as-deposited sample), S is positive. This indicate that the predominant charge carriers are positive holes, i.e. that all the as-deposited and annealed Mg-doped $CuCrO_2$ films are p-type semiconductors.

The S value for as-deposited sample is about 800 $\mu V.K^{-1}$. With the increase in annealing temperature up to 600 °C, the S value drastically decreases down to about 110 $\mu V.K^{-1}$. For higher annealing temperatures (T > 600°C), S slightly increases up to about 130 $\mu V.K^{-1}$. These Seebeck values are similar or lower than those reported in the literature for $CuCrO_2$ and Mg-doped $CuCrO_2$ due to the particular sensibility of S towards the Mg doping level and the thermal treatment (29; 31; 32; 58). The evolution of S is in agreement with the evolution of the electrical conductivity: the lowest Seebeck coefficient is obtained for the highest electrical conductivity σ in agreement with the Jonker's relation (59).

In non-degenerate semiconductor, S and ln σ are reliable by an affine relation. A plot of S versus ln σ, called a Jonker's plot, will have a slope of k_B/q (-86.15 $\mu V.K^{-1}$ for p-type characteristics). In the case of the Mg-doped $CuCrO_2$ films, Jonker's plot (shown in insert Figure 6 for the 100 nm thick samples) can be admittedly fitted with an affine relation, but with a 10 times smaller slope. It then confirms that the carrier transport behavior does not follow a classical non-degenerate model and is probably in favor of the hopping transport mechanism for degenerate semiconductor.

From the Seebeck coefficient measurement, it was possible to estimate the carrier concentration according to a Heikes formalism adapted for degenerate p-type semiconductors (60-62) with a carrier hopping mechanism only in between the Cu^+/Cu^{2+} species present on the copper crystallographic site. In this case, the adapted Heikes formula is equal to the following Equation 2:

$$S = +\frac{k_B}{q} \ln\left[\left(\frac{g1}{g2}\right)\frac{[Cu^+]}{[Cu^{2+}]}\right] \qquad \text{(Equation 2)}$$

where S is the experimental Seebeck coefficient (we suppose that S is saturated according to the Seebeck variation with the temperature mentioned in the literature for the 3% Mg-doped $CuCrO_2$ (41)), k_B is the Boltzmann constant, q is the charge of the carrier, g1 and g2 are the electron degeneracy of the Cu^+ and Cu^{2+} respectively and $[Cu^+]$ the Cu^+ proportion ($[Cu^{2+}] = 1 - [Cu^+]$). The $3d^{10}$ Cu^+ ion shows a coordination number of two in the delafossite structure with a total spin of zero with only one orbital configuration. The electron degeneracy of the Cu^+ is then equal to g1 = (2 × 0 + 1) x 1 = 1. In the case of Cu^{2+}, the octahedral environment is preferred to the tetrahedral one (40; 63), the electronic configuration is $3d^9$ and the spin is equal to ½ with two orbital configurations. The electron degeneracy of the Cu^{2+} is then equal to g2 = (2 × ½ + 1) x 2 = 4.

Finally, for a S = 114 $\mu V.K^{-1}$ obtained in the case of the 100 nm thick film annealed at 600 °C, the proportion of Cu^+ is estimated to 0.937 and consequently the complementary Cu^{2+} is 0.062 which corresponds to x + δ in the $(Cu^+_{1-x-2\delta}Cu^{2+}_{x+\delta})(Fe^{3+}_{1-x}Mg^{2+}_{x})O_{2+\delta}$ formulae. This latest value makes sense with the Mg doping level (x = 0.03) and the very limited oxygen intercalation into the $CuMO_2$ delafossite with small M-cations such as Fe (64) or Cr (40). The density of the total copper sites in the delafossite structure is equal to 2.32×10^{22} cm^{-3} (site 3a (Figure 1b) of the rhombohedral $R\bar{3}m$ space group in hexagonal axes setup, and for a total unit cell volume V = 129.36 $Å^3$ determined by GIXRD). As each Cu^{2+} could generate a hole in the valence band, we can conclude that the hole density (determined from the S measurement) h_S is equal to $0.062 \times 2.32\ 10^{22} = 1.45\ 10^{21}$ cm^{-3} in this condition. The estimated carrier concentrations are exposed in the Table 2 for every annealing temperature. They are once again in agreement with the AC Hall measurements (34) and the theoretical studies (65) exposed in the literature.

Optical properties: Optical spectra reported in Figure 7 show the evolution of the integrated Total Transmittance (TT), Total Reflectance (TR) and calculated Total Absorbance (TA = 1 - TT - TR) in the 300 to 1100 nm wavelength range domain and for the 100 nm thick films annealed at different temperatures. The TT and TR spectra of thin films are highly reproducible for identical thickness and thermal treatment.

The TT spectra show an increase of the average integrated total transmittance <TT> in the 400 to 800 nm visible range from 46 % to 69 % when the annealing temperature increase from 450 to 800 °C respectively (insert of Figure 7a). Any notable variation of the reflectance is observed (Figure 7b). The optical gap have been calculated by the direct band gap Tauc's relation (50) employed from the integrated transmittance data. The optical gap increases with the annealing temperature until a maximum value of Eg = 3.3 eV as shown in insert of Figure 7c. This maximal Eg value corresponds to the stabilized structure gap energy obtained for the optimal annealing temperature (600 °C) in good agreement with the previous structural and microstructural analyses. Eg = 3.3 eV obtained for Mg-doped $CuCrO_2$ films is just larger than those reported in the literature for various un-doped $CuCrO_2$ phase (from 3.05 to 3.20 eV depending on the deposition technique and thermal treatment (47; 49-51; 58; 67)). This slight increase of the gap energy is correlated to the slight increase of acceptors levels in the forbidden band according to the Burnstein-Moss effect (68). It's consistent with the Mg insertion in the delafossite structure as already reported in the literature (19; 56).

Opto-electrical properties: TT and TR spectra were fitted simultaneously using the SCOUT software (43) thank to dielectric models, which integrate a Kramer Kronig relation for interband transition (69) and Drude and Kim oscillator (70). The Kramer Kronig relation model incorporates a strength oscillator and the gap energy (which is approached by the experimental data obtained from the spectra). Kim oscillator integrates the resonance frequency, oscillator strength and damping parameters. From the Drude model, the dielectric carrier contribution is calculated from the plasma frequency and the carrier damping parameter. The total film thickness is initially set to the experimental value determined by mechanical profilometry and confirmed by X-ray reflectometry.

The refinement of these seven adjustable parameters (strength oscillator, gap energy, resonance frequency, oscillator strength, damping, plasma frequency and carrier damping) as well as the adjustment of the total thickness, permit to obtain a good fit of the experimental TT and TR spectra simultaneously. The satisfactory refinement of the dielectric model from optical data was initially obtained on the thicker film (≈ 300 nm) and validate just by thickness adjustment on the thinner one (≈ 300 nm). An example of TT and TR fits for the 300 nm Mg-doped $CuCrO_2$ film annealed at 600 °C are reported in Figure 7d. The standard deviation of the TT and TR spectra simultaneously fit is less than 4.4×10^{-4} (1.2×10^{-4} for TT and 3.2×10^{-4} for TR respectively).

Within these optical measurements, the hole density (h_{Opt}) and carrier mobility (μ_{Opt}) and then the corresponding equivalent conductivity (σ_{Opt}) can de deduced from the refined plasma frequency (Ω_p) and carrier damping (Ω_τ) parameters according to the following Equation 3 and Equation 4 respectively:

$$h_{Opt} = \frac{4\pi^2 c^2 \varepsilon_0 m^*}{q^2}\Omega_p^2 \qquad \text{(Equation 3)}$$

$$\mu_{Opt} = \frac{q}{2\pi c m^*}\frac{1}{\Omega_\tau} \qquad \text{(Equation 4)}$$

where c is the speed of light, ε_0 the vacuum permittivity, q the charge of the carrier and m* the hole effective mass. m* = 2.5 m_{e-} found in the literature (71) has been used. In addition to the electrical data, the optical refined (Ω_p and Ω_τ) and deduced (h_{Opt}, μ_{Opt} and σ_{Opt}) parameters are reported in Table 2 for the 300 nm thick film at different annealing temperatures.

The electrical characteristics deduced from the optical simulation show slightly higher carrier concentrations (h_{Opt}) than those estimated in this work by Seebeck measurements (h_{Elect}) and in the literature by AC Hall measurements (34). One can note that such high carrier concentrations h_{Opt} of about 10^{21} cm^{-3} has already been reported by Obulapathi et al. (72) on similar $CuCrO_2$ films. A lower value of the carrier concentration determined by Seebeck measurement (h_{Elect}) than those estimated by optical data (h_{Opt}), and then a lower measured conductivity than σ_{Opt}, could be due to the trapping of some carriers in the various defects as grain boundaries and/or surface traps. All the annealed samples also exhibit very low mobility (μ_{Opt} < 0.4 $cm^2.V^{-1}.s^{-1}$) in good accordance with strongly correlated system (hopping mechanism) and previous reports (15).

All the electrical characteristics (S, h_{Elect}, h_{Opt}, σ, σ_{Opt}) evolve in a same way and exhibit an optimal value for the 600 °C annealing sample. This 600 °C annealed sample is still the most optimized p-type TCO sample with a maximum value of Factor Of Merit (FOM) which also takes into account the optical properties. For the 600 °C annealing sample, FOM reaches 1.5×10^{-7} Ω^{-1} according to FOM = $<TT>^{10} / R_{\square}$ defined by Haacke **(**73**)** where $R_{\square}$ (Ω) is the sheet resistance of the film and <TT> the average total transmittance of the film in the 400 to 800 nm range. This FOM value is higher than FOM = 3.2×10^{-8} Ω^{-1} and FOM = 4.2×10^{-8} Ω^{-1} obtained for instance by Nagarajan et al. (15) (σ = 220 $S.cm^{-1}$ and <TT> = 30 % for a 250 nm thick film of $CuCr_{0.95}Mg_{0.05}O_2$) and Li et al. (74) (σ = 0.33 $S.cm^{-1}$ and <TT> = 63 % for a 127 nm thick film of $CuCrO_2$).

Optical index: Although the refractive index n is one of the most basic optical properties, its determination has never been reported for Mg-doped $CuCrO_2$ materials up to our knowledge. More generally, only few determinations of delafossite have been reported so far (75; 76) and often derived from reflectivity measurements (74; 77). Here, the Mg-doped $CuCrO_2$ complex index of refraction (n, k) were measured by spectroscopic ellipsometry (SE) and compared to those determined from the refinement of the optical data and those obtained using the envelop methods (78). For the determination of the complex index of refraction (n and k) by ellipsometry, the data were fitted with a model consisting of three layers: a quartz substrate, the delafossite film, and a surface roughness layer. The latter was modeled with a layer constituted of a mixture of 50 % Mg-doped $CuCrO_2$ and 50 % void according to the Bruggeman effective medium approximation (BEMA) (79). Figure 8a shows the fitting of ellipsometric data, I_s (sin $2\Psi \times \sin \Delta$) and I_c (sin $2\Psi \times \cos \Delta$) modeled with Tauc-Lorentz dispersion relations (80) for the 300 nm thick Mg-doped $CuCrO_2$ film annealed at 600 °C. The goodness of the fit can be estimated by the value of the mean square error value χ^2. In our case a low value of χ^2 has been obtained (χ^2 = 2.93). The fitting results indicated that the thickness of the film was 286.7 ± 0.9 nm and that the surface roughness layer was 6.8 ± 0.2 nm, i.e. a total thickness of 293.5 ± 1.1 nm in agreement with the previous measurements done by profilometry and X-ray reflectometry. The evolution of n and k in the range 350-1000 nm, which have been deduced from the ellipsometric model, is presented in the Figure 8b. The value of n ≈ 2.4 at 1000 nm in wavelength can be put forward, which is quite similar to those obtained at a wavelength of 1100 nm on $CuAlO_2$ single crystal (n = 2.32) and $CuInO_2$ (n = 2.1) by optical methods (75; 76) and ab-initio calculation (81). At the opposite, this value is really different from n = 1.2 at 650 nm announced by Li et al. (74) for $CuCrO_2$ which seems to be unrealistic given the delafossite electronic structure.

The refinement of the dielectric model from optical data was also used to determine the material susceptibility and then permits to calculate the complex index of refraction (n, k) as a function of the wavelength. Figure 8b compare the optical constants (n, k) determined by ellipsometry, refinement of the optical data and the envelop methods. Even if the complementary values of n estimated from spectrophotometry are slightly under those deduced from SE data due to the use of different techniques and models, these optical refractive index values remains however in the same range.

Conclusions

This work provides insight to the delafossite Mg-doped $CuCrO_2$ thin film deposition and opto-electronic properties. It offers complete structural, microstructural, electrical and optical characterizations helpful for the understanding and optimization of technologically relevant p-type TCO materials.

The Mg-doped $CuCrO_2$ thin films were deposited on quartz substrate by magnetron sputtering from homemade ceramic target, then annealed at various temperatures for 4 h under vacuum in the 450 to 800 °C range. The structural characterization shows an increase in the delafossite crystallinity with the annealing temperature. The limited and controlled oxygen loss during the deposition and annealing processes assists in the formation of the delafossite phase without any particular *(00l)* preferred orientation in the limit of the reduction of Cu(I) species into metallic copper nanoparticles.

The microstructural analysis emphasizes a very weak surface roughness for the as-deposited film and highlights a particular microstructural evolution versus annealed temperature with a rupture in crystallite growth at about 600 °C. This temperature was evidenced as optimal temperature for the p-type TCO properties.

Different characterization methods were used to determine the carrier concentration in Mg-doped $CuCrO_2$ thin films. DC Hall measurement has not permitted to estimate a carrier density, whereas the Seebeck measurement allows us to justify the positive holes as predominant charge carriers and estimate the effective carrier concentration of about 10^{21} cm^{-3} with the hopping transport formalism. Measurement of transmittance and reflectance associated to a dielectric model corroborated these values. These optical measurements also allowed to determine for the first time the refractive index (n, k) of Mg-doped $CuCrO_2$. A value of n = 2.3 at 1100 nm was obtained, which is closed to those of most of other copper delafossites. Spectroscopic ellipsometry confirmed the order of magnitude of refractive index and extinction coefficient deduced from the transmittance and reflectance spectra. The optimal TCO properties of the Mg-doped $CuCrO_2$ thin films are obtained for a 100 nm thick after a 600 °C for 4 h under vacuum treatment. It shows an electrical conductivity of σ = 1.4 $S.cm^{-1}$ and an average transmittance of 63 % in the visible range. The Haacke's factor of merit of this Mg-doped $CuCrO_2$ thin films is equal to 1.5×10^{-7} Ω^{-1}. This result is one of the best FOM value reported to date for p-type TCO material. Moreover, it was obtained for films processed at moderate temperature. Accordingly, rf-sputtered Mg-doped $CuCrO_2$ thin films show promising results for future transparent electronic devices conception.

ACKNOWLEDGMENT

The authors gratefully acknowledge the support of Institut Carnot CIRIMAT (bourse de these Carnot M. Lalanne), the Fédération de Recherche FERMAT (Temperature XRD and PVE measurements) and the French RENATECH network through Institut Carnot LAAS (ellipsometry measurements).

REFERENCES

(1) A. Stadler; Transparent Conducting Oxides - An up-to-date overview. *Materials* **2012**, *5,* 661-683.

(2) L. Castaneda; Present status of the development and application of Transparent Conductors Oxide thin solid films. *Materials Sciences and Applications* **2011**, *2,* 1233-1242.

(3) D.S. Ginley; C. Bright; Transparent conducting oxides. *Materials Research Society Bulletin* **2000**, *8,* 15-18.

(4) H. Kawazoe; M. Yasukawa; H. Hyodo; M. Kurita; H. Yanagi; H. Hosono; P-type electrical conduction in transparent thin films of $CuAlO_2$. *Nature* **1997,** *389,* 939-942.

(5) R. Seshadri; C. Felser; K. Thieme; W. Tremel; Metal-metal bonding and metallic behavior in some ABO_2 delafossites. *Chemistry of Materials* **1998,** *10,* 2189-2196.

(6) H. Yanagi; S.Park; A. Draeseke; D. Keszler; J. Tate; P-type conductivity in transparent oxides and sulfide fluorides. *Journal of Solid State Chemistry* **2003,** *175,* 34-38.

(7) A.N. Banerjee; K.K. Chattopadhyay; Recent developments in the emerging field of crystalline p-type transparent conducting oxide thin films. *Progress in Crystal Growth and Characterization of Materials* **2005,** *50,* 52-105.

(8) S. Sheng; G. Fang; C. Li; S. Xu; X. Zhao; P-type transparent conducting oxides. *Physica Status Solidi A : Applications and Material Science* **2006,** *203,* 1891-1900.

(9) B. Ingram; G. Gonzalez; T. Mason; D. Shahriari; A. Barnabé; D. Ko; P. Poeppelmeier; Transport and defect mechanisms in cuprous delafossites. 1. Comparison of hydrothermal and standard solid-state synthesis in $CuAlO_2$. *Chemistry of Materials* **2004,** *16,* 5616-5622.

(10) H. Kawazoe; H. Yanagi; K. Ueda; H. Hosono; Transparent p-type conducting oxides: design and fabrication of p-n heterojunctions. *Materials Research Society Bulletin* **2000,** *8,* 28-36.

(11) J. Tate; M. Jayaraj; A. Draeseke; T. Ulbrich; A. Sleight; K. Vanaja; R. Nagarajan; J. Wager; R. Hoffman; P-Type oxides for use in transparent diodes. *Thin Solid Films* **2002,** *411,* 119-124.

(12) H. Yanagi; T. Hase; S. Ibuki; K. Ueda; H. Hosono; Bipolarity in electrical conduction of transparent oxide semiconductor $CuInO_2$ with delafossite structure. *Applied Physics Letters* **2001,** *78,* 1583-1585.

(13) M. Jayaraj; A. Draeseke; J. Tate; A. Sleight; P-Type transparent thin films of $CuY_{1-x}Ca_xO_2$. *Thin Solid Films* **2001,** *397,* 244-248.

(14) Y. Kakehi; K. Satoh; T. Yotsuya; A. Ashida; T. Yoshimura; N. Fujimura; Electrical and optical properties of excess oxygen intercalated $CuScO_2$ (0001) epitaxial films prepared by oxygen radical annealing. *Thin Solid Films* **2008,** *516,* 5785-5789.

(15) R. Nagarajan; A. Draeseke; A. Sleight; J. Tate; P-type conductivity in $CuCr_{1-x}Mg_xO_2$ films and powders. *Journal of Applied Physics* **2001,** *89,* 8022-8025.

(16) G. Thomas; Invisible circuits. *Nature* **1997,** *389,* 907-908.

(17) J. Wager; D. Kesler; D. Presley; Transparent Electronics. Springer Edition, **2008**.

(18) A. Barnabé; E. Mugnier; L. Presmanes; P. Tailhades; Preparation of delafossite $CuFeO_2$ thin films by rf-sputtering on conventional glass substrate. *Materials Letters* **2006,** *60,* 3468-3470.

(19) X. Li; M. Han; X. Zhang; C. Shan; Z. Hu; Z. Zhu; J. Chu; Temperature-dependent band gap, interband transitions, and exciton formation in transparent p-type delafossite $CuCr_{1-x}Mg_xO_2$ films. *Physical Review B* **2014**, *90*, 035308.

(20) T. Chiu; Y. Yang; A. Yeh; Y. Wang ; Y. Feng ; Antibacterial property of $CuCrO_2$ thin films prepared by RF magnetron sputtering deposition. *Vacuum* **2013***, 87*, 174-177.

(21) R. Rao; A. Dandekar; R. Baker; M. Vannice; Properties of copper chromite catalysts in hydrogenation reactions. *Journal of Catalysis* **1997**, *171*, 406-419.

(22) A. Amrute; G. Larrazábal; C. Mondelli; J. Pérez-Ramírez; $CuCrO_2$ Delafossite: a stable copper catalyst for chlorine production. *Angewandte Chemie* **2013**, *52*, 9772-9775.

(23) P. Zhang; Y. Shi; M. Chi; J. Park; G. Stucky; E. McFarland; L. Gao; Mesoporous delafossite $CuCrO_2$ and spinel $CuCr_2O_4$: synthesis and catalysis. *Nanotechnology* **2013**, *24*, 345704.

(24) S. Saadi; A. Bouguelia; M. Trari; Photocatalytic hydrogen evolution over $CuCrO_2$. *Solar Energy* **2006**, *80*, 272-280.

(25) T. Okuda; T. Onoe; Y. Beppu; N. Terada; T. Doi; S. Miyasaka; Y. Tokura; Magnetic and transport properties of delafossite oxides $CuCr_{1-x}(Mg,Ca)_xO_2$. *Journal of Magnetism and Magnetic Materials* **2007**, *310*, 890-892.

(26) A. Maignan; C. Martin; R. Frésard; V. Eyert; E. Guilmeau; S. Hébert; M. Poienar; D. Pelloquin; On the strong impact of doping in the triangular antiferromagnet $CuCrO_2$. *Solid State Communications* **2009,** *149,* 962-967.

(27) M. Poienar; F. Damay; C. Martin; V. Hardy; A. Maignan ; G. Andre; Structural and magnetic properties of $CuCr_{1-x}Mg_xO_2$ by neutron powder diffraction. *Physical Review B* **2009***, 79*, 014412.

(28) T. Okuda; N. Jufuku; S. Hidaka; N. Terada; Magnetic, transport, and thermoelectric properties of the delafossite oxides $CuCr_{1-x}Mg_xO_2$ ($0 \leq x \leq 0.04$). *Physical Review B* **2005**, *72*, 144403.

(29) Y. Ono; K. Satoh; T. Nozaki; T. Kajitani; Structural, magnetic and thermoelectric properties of delafossite-type oxide; $CuCr_{1-x}Mg_xO_2$ ($0 \leq x \leq 0.05$). *Japanese Journal of Applied Physics* **2007,** *46,* 1071-1075

(30) K. Hayashi; K. Sato; K. Nozaki ; T. Kajitani ; Effect of doping on thermoelectric properties of delafossite-type Oxide $CuCrO_2$. *Japanese Journal of Applied Physics* **2008***, 57*, 59-63.

(31) E. Guilmeau; M. Poinar; S. Kremer; S. Marinel; S. Hébert; R. Frésard; A. Maignan; Mg Substitution in $CuCrO_2$ delafossite compounds. *Solid State Communication* **2011,** *23,* 1798.

(32) Q. Meng; S. Lu; S. Lu; Y. Xiang; Preparation of p-type $CuCr_{1-x}Mg_xO_2$ bulk with improved thermoelectric properties by sol-gel method. *Journal of Sol-gel Science and Technology* **2012,** *63,* 1-7.

(33) M. Soda; K. Kimura; T. Kimura; K. Hirota; Domain rearrangement and spin-spiral-plane flop as sources of magnetoelectric effects in delafossite $CuCrO_2$. *Physical Review B* **2010**, *81*, 100406.

(34) M. O'Sullivan ; P. Stamenov; J. Alaria; M. Venkatesan; J. M. D. Coey; Magnetoresistance of $CuCrO_2$-based delafossite films; *Journal of Physics : Conference Series* **2010,** *200,* 052021.

(35) S. Zhou; X. Fang; Z. Deng; D. Li; W. Dong; R. Tao; G. Meng; T. Wang; Room temperature ozone sensing properties of p-type $CuCrO_2$ nanocrystals. *Sensors and Actuators B* **2009**, *143*, 119-123.

(36) D. Xiong; Z. Xu; X. Zeng; W. Zhang; W. Chen; X. Xu; M. Wang ; Y. Cheng ; Hydrothermal synthesis of ultrasmall $CuCrO_2$ nanocrystal alternatives to NiO nanoparticles in efficient p-type dye-sensitized solar cells. *Journal of Materials Chemistry* **2012**, *22*, 24760-24768.

(37) J. Shu; X. Zhu ; T. Yi ; $CuCrO_2$ as anode material for lithium ion batteries. *Electrochimica Acta* **2009***, 54*, 2795-2799.

(38) M.J. Han; Z.H. Duan; J.Z. Zhang; S. Zhang; Y.W. Li; Z.G. Hu; J.H. Chu; Electronic transition and electrical transport properties of delafossite $CuCr_{1-x}Mg_x$ O_2 ($0 \leq x \leq 12\%$) films prepared by the sol-gel method: A composition dependence study. *Journal of Applied Physics* **2013**, *114*, 163526.

(39) M. Lalanne; M. Demont; A. Barnabé; AC conductivity and dielectric properties of $CuFe_{1-x}Cr_xO_2$:Mg delafossite. *Journal of Physics D: Applied Physics*, **2011**, *44*, 185401

(40) M. Lalanne; A. Barnabé; F. Mathieu; P. Tailhades; Synthesis and thermostructural studies of a $CuFe_{1-x}Cr_xO_2$ Delafossite solid solution with $0 \leq x \leq 1$. *Inorganic Chemistry* **2009,** *48,* 6065-6071.

(41) E. Mugnier; A. Barnabé; L. Presmanes; P. Tailhades; Thin films preparation by rf-sputtering of copper/iron ceramic targets with Cu/Fe=1: From nanocomposites to delafossite compounds. *Thin Solid Films* **2008,** *516,* 1453-1456.

(42) D. Necas; P. Klapetek; Gwyddion data analysis software. http://gwyddion.net/

(43) W. Theiss; Hard & Software. http://www.mtheiss.com/

(44) K. Tonooka; N. Kikuchi; Preparation of transparent $CuCrO_2$:Mg/ZnO p-n junctions by pulsed laser deposition. *Thin Solid Films* **2006,** *515,* 2415-2418.

(45) S. Götzendörfer; C. Polenzky; S. Ulrich; P. Löbmann; Preparation of p-type conducting transparent $CuCrO_2$ and $CuAl_{0.5}Cr_{0.5}O_2$ thin films by sol–gel processing. *Journal of Sol-Gel Science and Technology* **2009,** *52,* 113-119.

(46) R. Bywalez; S. Götzendoerfer; P. Loebmann; Structural and physical effects of Mg-doping on p-type $CuCrO_2$ and $CuAl_{0.5}Cr_{0.5}O_2$ thin films. *Journal of Materials Chemistry* **2010,** *20,* 6562-6570.

(47) H. Chen; W. Yang; K. Chang; Characterization of delafossite-$CuCrO_2$ thin films prepared by post-annealing using an atmospheric pressure plasma torch. *Applied Surface Science* **2012,** *258,* 8775-8779.

(48) T. Chiu; S. Tsai; Y. Wang; K. Hsu; Preparation of p-type conductive transparent $CuCrO_2$:Mg thin films by chemical solution deposition with two-step annealing. *Ceramics International* **2012,** *48,* S673-S676.

(49) D. Li; X. Fang; A. Zhao; Z. Deng; W. Dong; T. Tao; Physical properties of $CuCrO_2$ films prepared by pulsed laser deposition. *Vacuum* **2010,** *84,* 851-856.

(50) S. Mahapatra; S. Shivashankar; Low-pressure metal-organic CVD of transparent and p-type conducting $CuCrO_2$ thin films with high conductivity. *Chemical Vapor Deposition* **2003,** *9,* 238-240.

(51) G. Dong; M. Zhang; X. Zhao; H. Yan; C. Tian; Y. Ren; Improving the electrical conductivity of $CuCrO_2$ thin film by N doping. *Applied Surface Science* **2010,** *256,* 4121-4124.

(52) V. Varadarajan; D.P. Norton; $CuGaO_2$ thin film synthesis using hydrogen-assisted pulsed laser deposition. *Applied Physics A* **2006,** *85,* 117-120.

(53) A. Barnabé; A. Chapelle; L. Presmanes; P. Tailhades; Copper and iron based thin film nanocomposites prepared by radio frequency sputtering. Part I: elaboration and characterization of metal/oxide thin film nanocomposites using controlled in situ reduction process. *Journal of Materials Science* **2013,** 48, 3386-3394.

(54) R.S. Yu; C.M. Wu; Characteristics of p-type transparent conductive $CuCrO_2$ thin films. *Applied Surface Science* **2013,** *282,* 92-97.

(55) T. Chiu; K. Tonooka; N. Kikuchi; Fabrication of ZnO and $CuCrO_2$: Mg thin films by pulsed laser deposition with in situ laser annealing and its application to oxide diodes. *Thin Solid Films* **2008,** *516,* 5941-5947.

(56) P. Sadik; M. Ivill; V. Craciun; D. Norton; Electrical transport and structural study of $CuCr_{1-x}Mg_xO_2$ delafossite thin films grown by pulsed laser deposition. *Thin Solid Films* **2009,** *517,* 3211-3215.

(57) A. C. Rastogi; S. H. Lim; S. B. Desu; Structure and optoelectronic properties of spray deposited Mg doped p-$CuCrO_2$ semiconductor oxide thin films. *Journal of Applied Physics* **2008,** *104,* 023712.

(58) R. Nagarajan; N. Duan; M. Jayaraj; J. Li; K. Vanaja; A. Yokochi; A. Draeseke; J. Tate; A. Sleight; P-type conductivity in the delafossite structure. *International Journal of Inorganic Materials* **2001,** *3,* 265-270.

(59) G. Jonker; The application of combined conductivity and Seebeck-effect plots for the analysis of semiconductor properties. *Philips Research Reports* **1968,** *23,* 131-138.

(60) R. R. Heikes; R. W. Ure; Thermoelectricity : Science and Engineering. Interscience **1961**.

(61) W. Ketir; S. Saadi; M. Trari; Physical and photoelectrochemical characterization of $CuCrO_2$ single crystal. *Journal of Solid State Electrochemistry* **2012,** *16,* 213-218.

(62) W. Koayashi; I. Terasaki; M. Mikami; R. Funahashi; Negative Thermoelectric Power Induced by Positive Carriers in $CaMn_{3-x}Cu_xMn_4O_{12}$. *Journal of the physical Society of Japan* **2004,** *73,* 523-525.

(63) A. Navrotsky; O.J. Kleppa; The thermodynamics of cation distributions in simple spinels. *Journal of Inorganic and Nuclear Chemistry* **1967,** *29,* 2701.

(64) E. Mugnier; A. Barnabé; P. Tailhades; Synthesis and characterization of $CuFeO_{2+\delta}$ delafossite powders. *Solid State Ionics* **2006,** *177,* 607-612.

(65) D. Scanlon; A. Walsh; G. W. Watson; Understanding the p-type conduction properties of the transparent conducting oxide $CuBO_2$: A Density Functional Theory Analysis. *Chemistry of Materials* **2009,** *21,* 4568-4576.

(66) J. Tauc; Optical properties and electronic structure of amorphous Ge and Si. *Materials Research Bulletin* **1968,** *3,* 37-46.

(67) D. Shin; J. Foord; R. Egdell ; A. Walsh ; Electronic structure of $CuCrO_2$ thin films grown on Al_2O_3(001) by oxygen plasma assisted molecular beam epitaxy. *Journal of Applied Physics* **2012***, 112*, 113718.

(68) E. Burnstein; Anomalous optical absorption limit in InSb, *Physical Review* **1954,** *93,* 3, 632-633.

(69) F. Demichelis; G. Kaniadakis; A. Tagliaferro; E. Tresso; New approach to optical analysis of absorbing thin solid films. *Applied Optics* **1987,** *26,* 1737.

(70) C.C. Kim; J. W. Garland; H. Abad; P.M. Raccah; Modeling the optical dielectric function of semiconductors: extension of the critical-point parabolic-band approximation. *Physical Review B* **1992,** *45,* 11749.

(71) G. Hautier; A. Miglio; G. Ceder; G-M. Rignanese; X. Gonze; Identification and design principles of low hole effective mass p-type transparent conducting oxides. *Nature Communication* **2013,** *4,* 2292.

(72) L. Obulapathi; A. GuruSampath Kumar; T. Sofi Saramash; D. Jhansi Rani; T. Subba Rao; Effect of Annealing temperature on structural, electrical and optical properties of $CuCrO_2$ thin films by reactive DC magnetron sputtering. *International Journal of Research in Pure and Applied Physics* **2014,** *4,* 16-19.

(73) G. Haacke; New figure of merit for transparent conductors. *Journal of Applied Physics* **1976,** 47, 4086E9.

(74) D. Li; X. Fang; A. Zhao; Z. Deng; W. Dong; R. Tao; Physical properties of $CuCrO_2$ films prepared by pulsed laser deposition. *Vacuum* **2010,** *84,* 851-856.

(75) J. Pellicer-Porres; A. Segura; D. Kim; Refractive index of the $CuAlO_2$ delafossite. *Semiconductor Science and Technology* **2009,** *24,* 015002.

(76) C. Teplin; T. Kaydanova; D. Young; J. Perkins; D. Ginley; A. Ode; D. Readey; A simple method for the preparation of transparent p-type Ca-doped $CuInO_2$ films: Pulsed-laser deposition from air-sintered Ca-doped Cu2In2O5 targets. *Applied Physics Letters* **2004,** *85,* 3789-3791.

(77) A. Banerjee; C. Ghosh; S. Das; K. Chattopadhyay; Electro-optical characteristics and field-emission properties of reactive DC-sputtered p-$CuAlO_{2+x}$ thin films. *Physica B* **2005,** *370,* 264-276.

(78) J. C. Manifacier; J. Gasiot; J. P. Fillard; A simple method for the determination of the optical constants n; k and the thickness of a weakly absorbing thin film. *Journal of Physics E : Scientific Instrument* **1976,** *9,* 1002-1004.

(79) D.A.G. Bruggeman; Berechnung verschiedener physikalischer Konstanten von heterogenen Substanzen I. Dielektrizitätskonstanten und Leitfähigkeiten der Mischkörper aus isotropen Substanzen. *Annalen der Physik* **1935,** *416,* 636-664.

(80) G.E. Jellison; F.A. Modine; Parameterization of the optical functions of amorphous materials in the interband region. *Applied Physics Letters* **1996,** *69,* 371-373. G.E. Jellison; F.A. Modine; Erratum: 'Parameterization of the optical functions of amorphous materials in the interband region'. *Applied Physics Letters* **1996,** *69,* 2137-2137.

(81) J. Pellicer-Porres; D. Martinez-Garcia; A. Segura; P. Rodriguez-Hernandez; A. Munoz; J.C. Chervin; N. Garro; D. Kim; Pressure and temperature dependence of the lattice dynamics of $CuAlO_2$ investigated by Raman scattering experiments and ab initio calculations. *Physical Review B* **2006,** *74,* 184301.

Table Caption

Table 1. Process parameters for the deposition of delafossite Mg-doped $CuCrO_2$ by rf-sputtering.

Table 2. Electrical (Seebeck coefficient S) and optical (TT and TR refined plasma frequency Ω_p and damping constant Ω_τ parameters) measurements and the corresponding carrier concentrations (h_{Elect} and h_{Opt}), mobility (μ_{Opt}) and the electrical conductivity (σ_{Opt}) of as-deposited and annealed 300 nm thick films.

Figure caption

Figure 1. a) XRD pattern of Mg-doped $CuCrO_2$ target. Traces of magnesiochromite are indicated by the ♦ symbol. b) Schematic representation of the delafossite structure.

Figure 2. XRD patterns of 300 nm thick Mg-doped $CuCrO_2$ films. a) In-situ TXRD patterns registered in θ-θ Bragg-Brentano geometry at various temperature in the range of 30 to 800 °C under primary vacuum and b) α = 1 ° GIXRD patterns registered at room temperature after similar ex-situ annealing treatment.

Figure 3. a) Cross section SEM and b) surface AFM micrographs of 300 nm thick as-deposited thin film. Corresponding c) 3D and d) surface AFM micrographs for a 100 nm thick as-deposited film.

Figure 4. AFM micrographs of 100 nm Mg-doped $CuCrO_2$ annealed at various temperatures in the range of 450 °C to 700 °C for 4 h under primary vacuum. Average particle size (D) and root mean square roughness (RMS) are indicated for all the samples.

Figure 5. a) Electrical conductivity σ of the 100 nm and 300 nm thin films for different annealing temperatures. Are also plotted on this graph some data from references (15; 25; 28; 35-36). b) Sheet resistance $R_{\square} = (\sigma.\text{thickness})^{-1}$ as a function of the thickness for films annealed at various temperatures.

Figure 6. The measured Seebeck coefficients (S) for 100 nm thick films annealed at different temperatures. Insert: Jonker's plot.

Figure 7. a) TT b) TR and c) TA optical spectra of 100 nm thin films deposited on quartz substrate and annealed at different temperatures. Pictures of these films treated at different temperatures and placed on a medium of patterned paper, are presented in insert a) to illustrate their transparency to natural white light. Values of the average total transmittance <TT> of the films in the 400 to 800 nm visible range are also reported in function of the annealing temperature in insert a). The direct optical gap calculated from the Tauc's relation in function of the annealing temperature is plotted in insert c). d) TT and TR optical spectra of a 300 nm thin film and the corresponding simulated TT and TR spectra.

Figure 8. 300 nm thick Mg-doped $CuCrO_2$ film annealed at 600 °C optical constants. a) experimental and simulated ellipsometric data I_s ($\sin 2\Psi \times \sin \Delta$) and I_c ($\sin 2\Psi \times \cos \Delta$) as a function of optical wavelength, and b) corresponding optical constants, n and k, as determined from analysis of ellipsometry data (green circles), and TT, TR data (refinement of the dielectric model in black full line and envelop method in dashed line).

Table 1

Target material	3%^{at} Mg-doped $CuCrO_2$
Substrate	Fused quartz
Power (W/cm^2)	0.9
Magnetron	Yes
Argon pressure P (Pa)	0.5
Target to substrate distance d (cm)	5

Table 2

	Electrical measurements		Optical measurements				
Annealing temperature T (°C)	**Seebeck Coefficient S ($\mu V.K^{-1}$)**	**Carrier concentration h_{Elect} (cm^{-3})**	**Plasma frequency Ω_p (cm^{-1})**	**Damping constant Ω_τ (cm^{-1})**	**Carrier concentration h_{Opt} (cm^{-3})**	**Carrier mobility μ_{Opt} ($cm^2.V^{-1}.s^{-1}$)**	**Electrical conductivity σ_{Opt} ($S.cm^{-1}$)**
as-deposited	804	$5.19\ 10^{17}$	15	1475	$6.30\ 10^{15}$	2.530	0.002
500	140	$1.09\ 10^{21}$	7353	50314	$1.50\ 10^{21}$	0.074	17.76
550	116	$1.42\ 10^{21}$	11812	36237	$3.90\ 10^{21}$	0.103	64.27
600	121	$1.34\ 10^{21}$	8741	24055	$2.13\ 10^{21}$	0.155	52.82
650	122	$1.32\ 10^{21}$	6645	19442	$1.23\ 10^{21}$	0.192	37.78
700	133	$1.18\ 10^{21}$	8597	22950	$2.00\ 10^{21}$	0.163	52.16
750	167	$8.07\ 10^{20}$	4372	9137	$5.30\ 10^{20}$	0.408	34.60

Figure 1

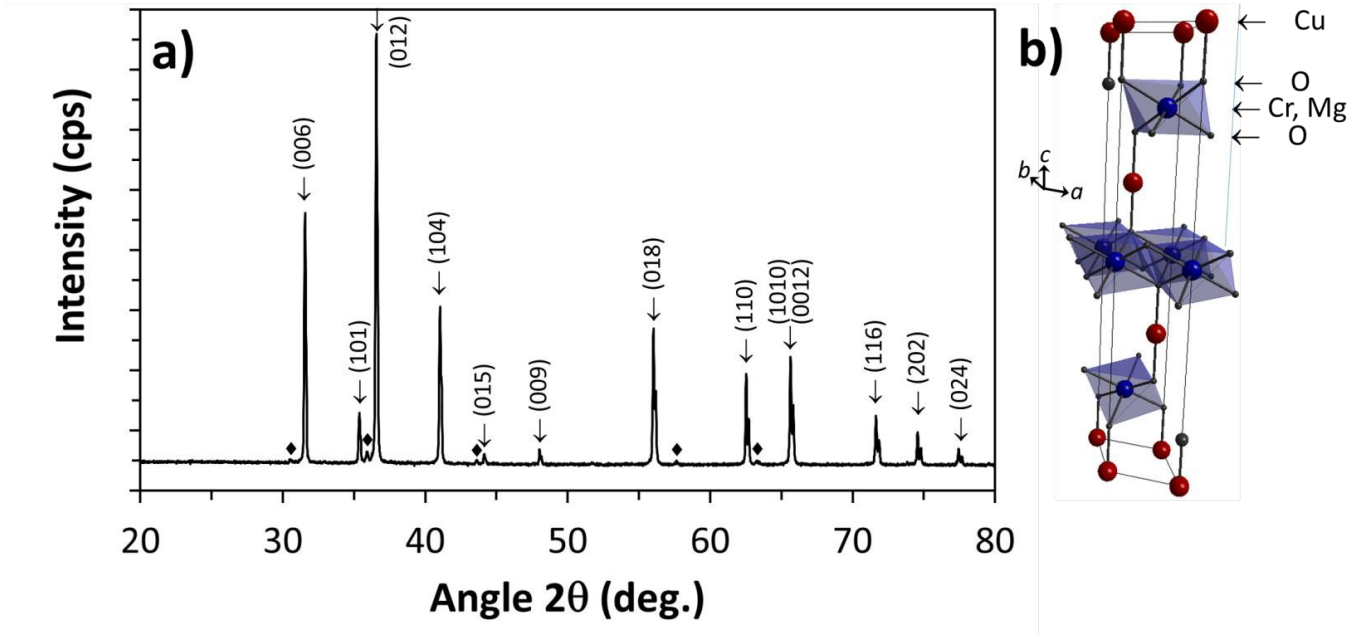

Figure 2

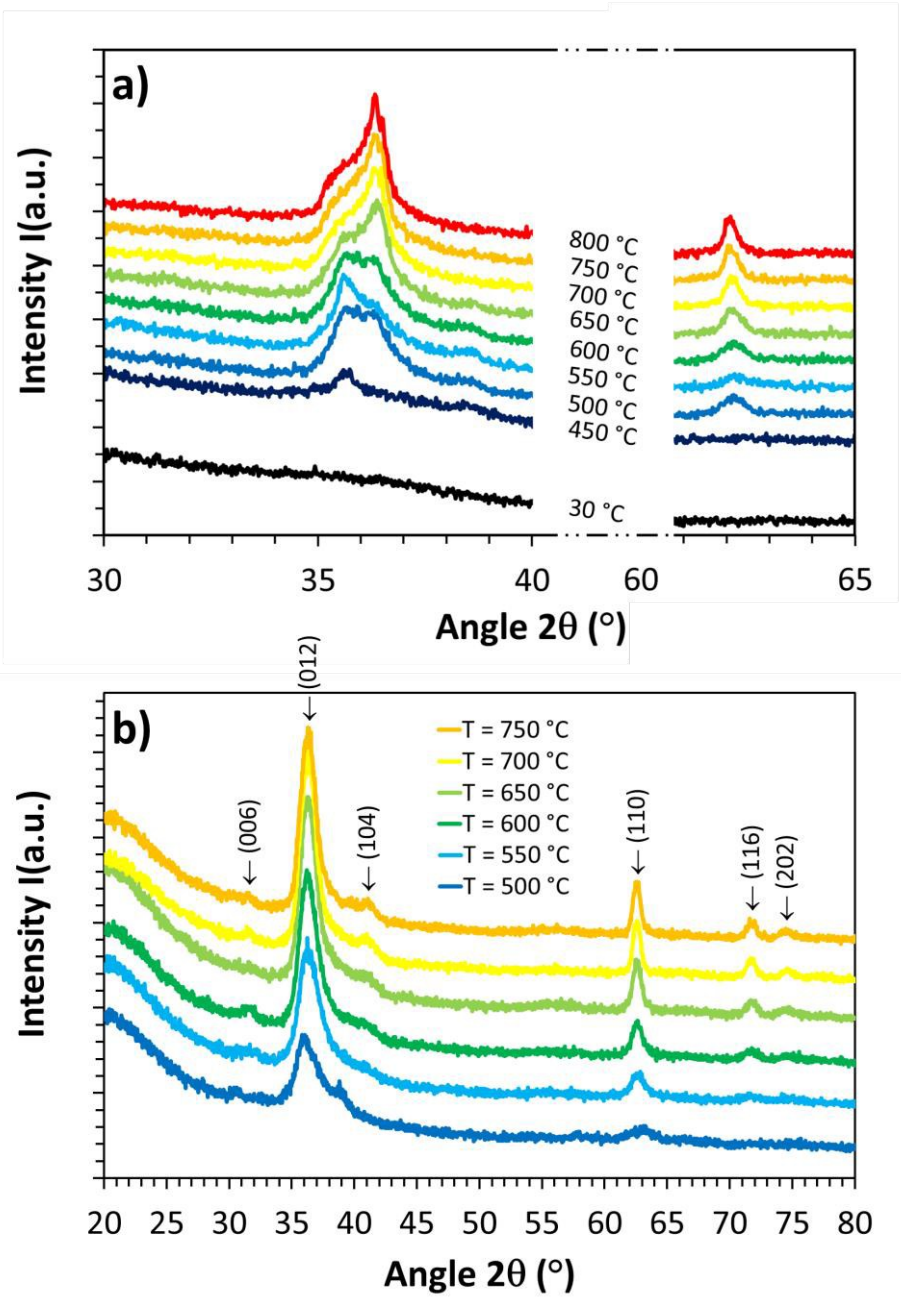

Figure 3

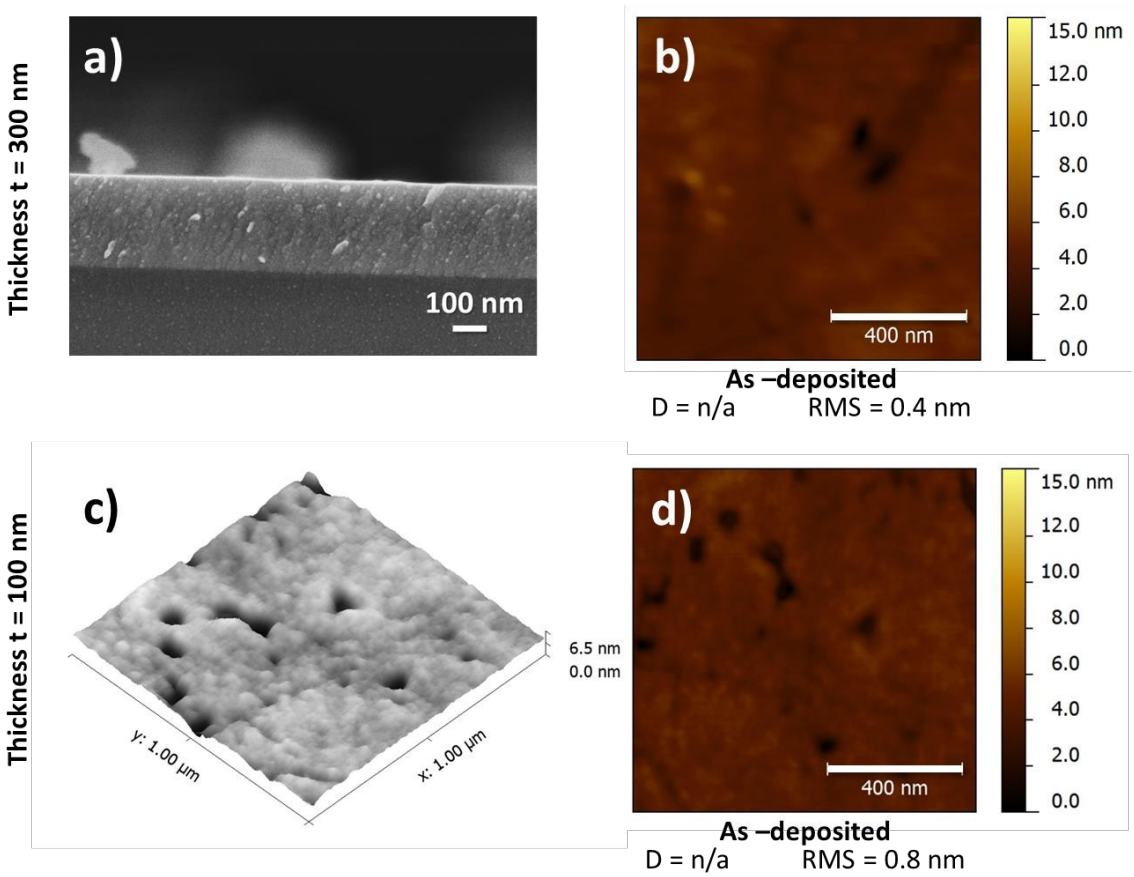

Figure 4

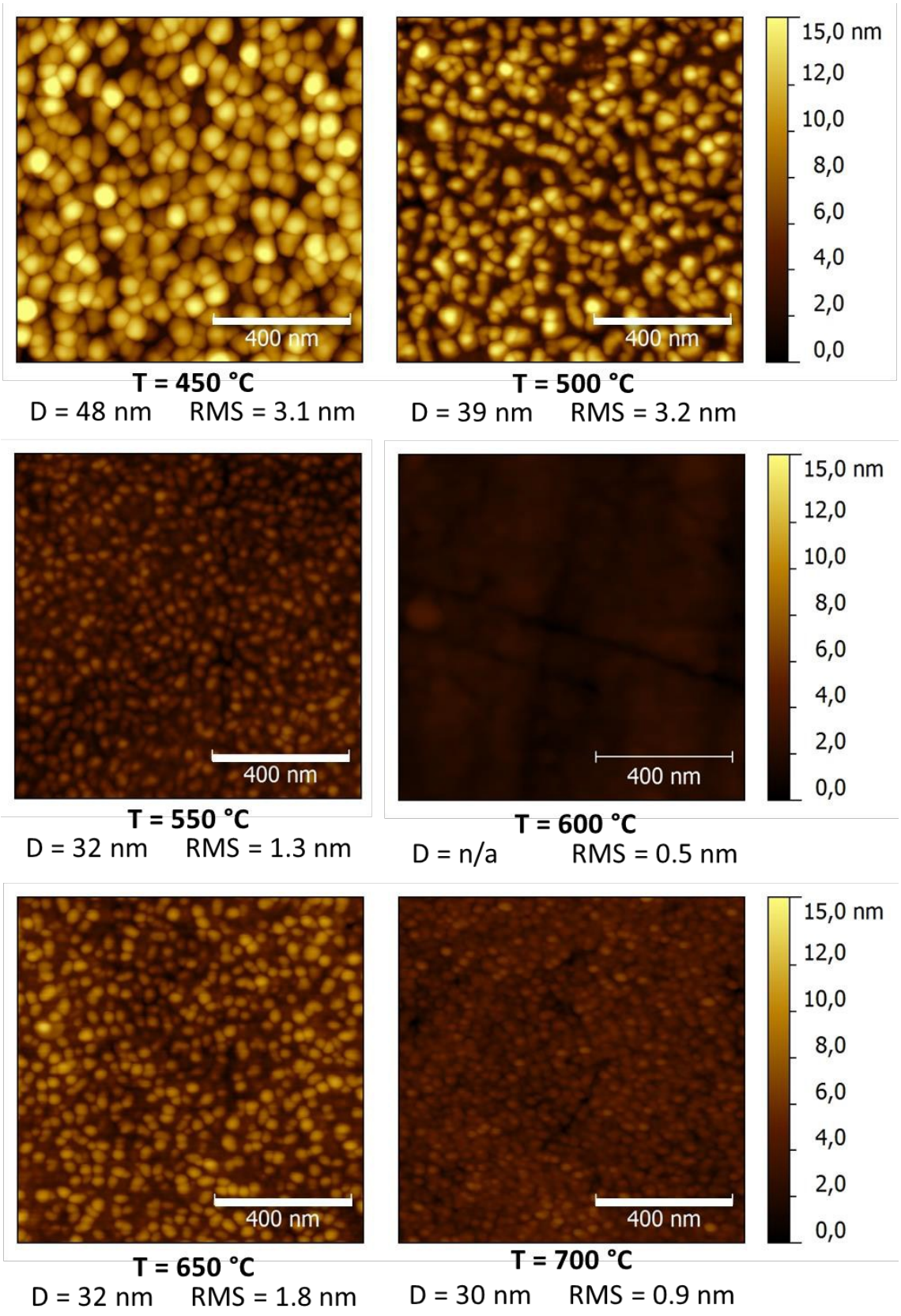

Figure 5

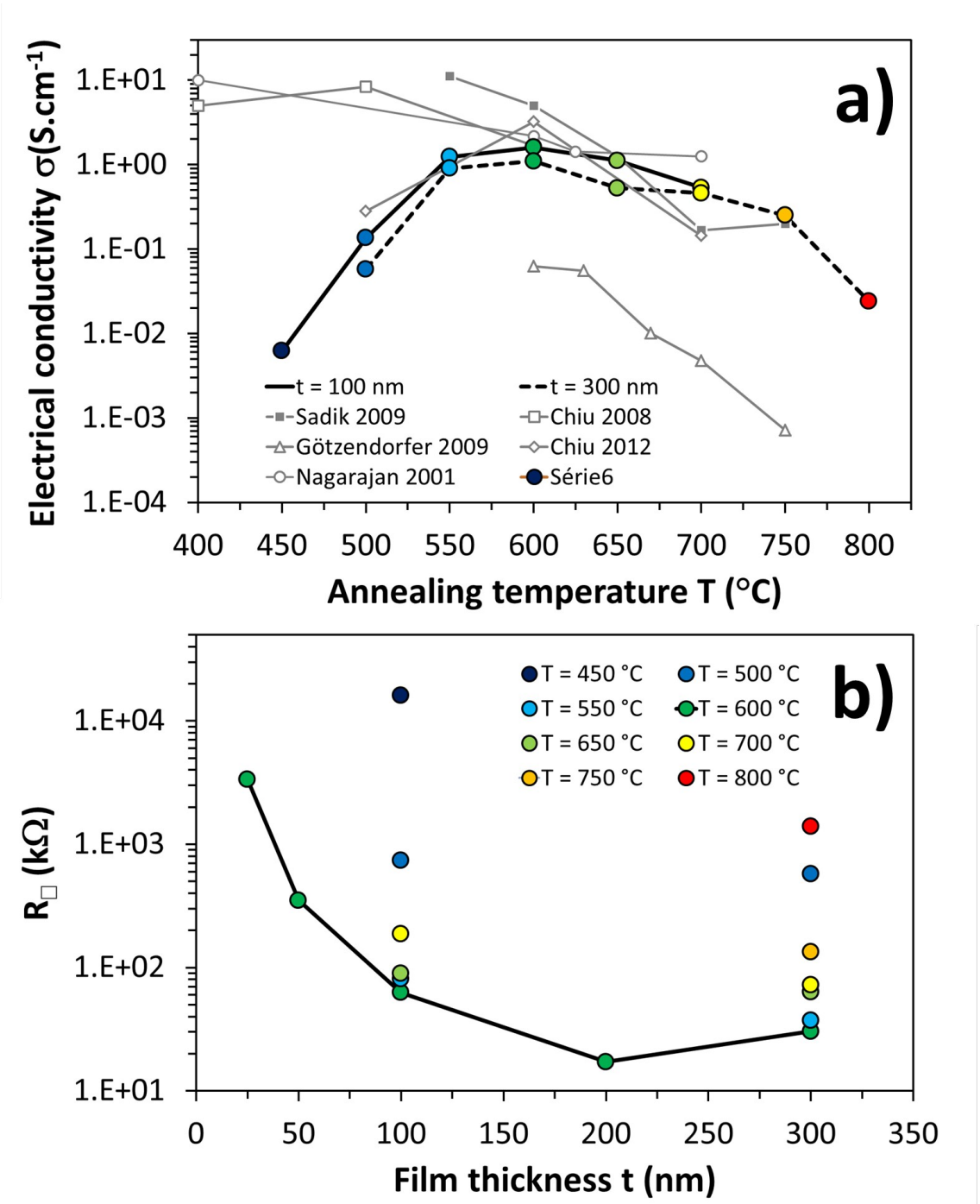

Figure 6

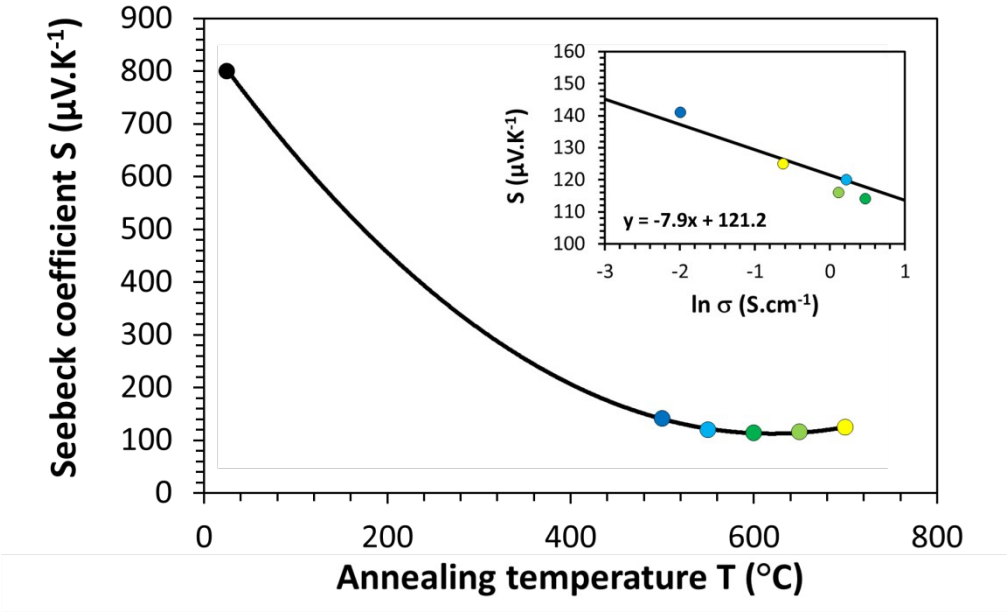

Figure 7

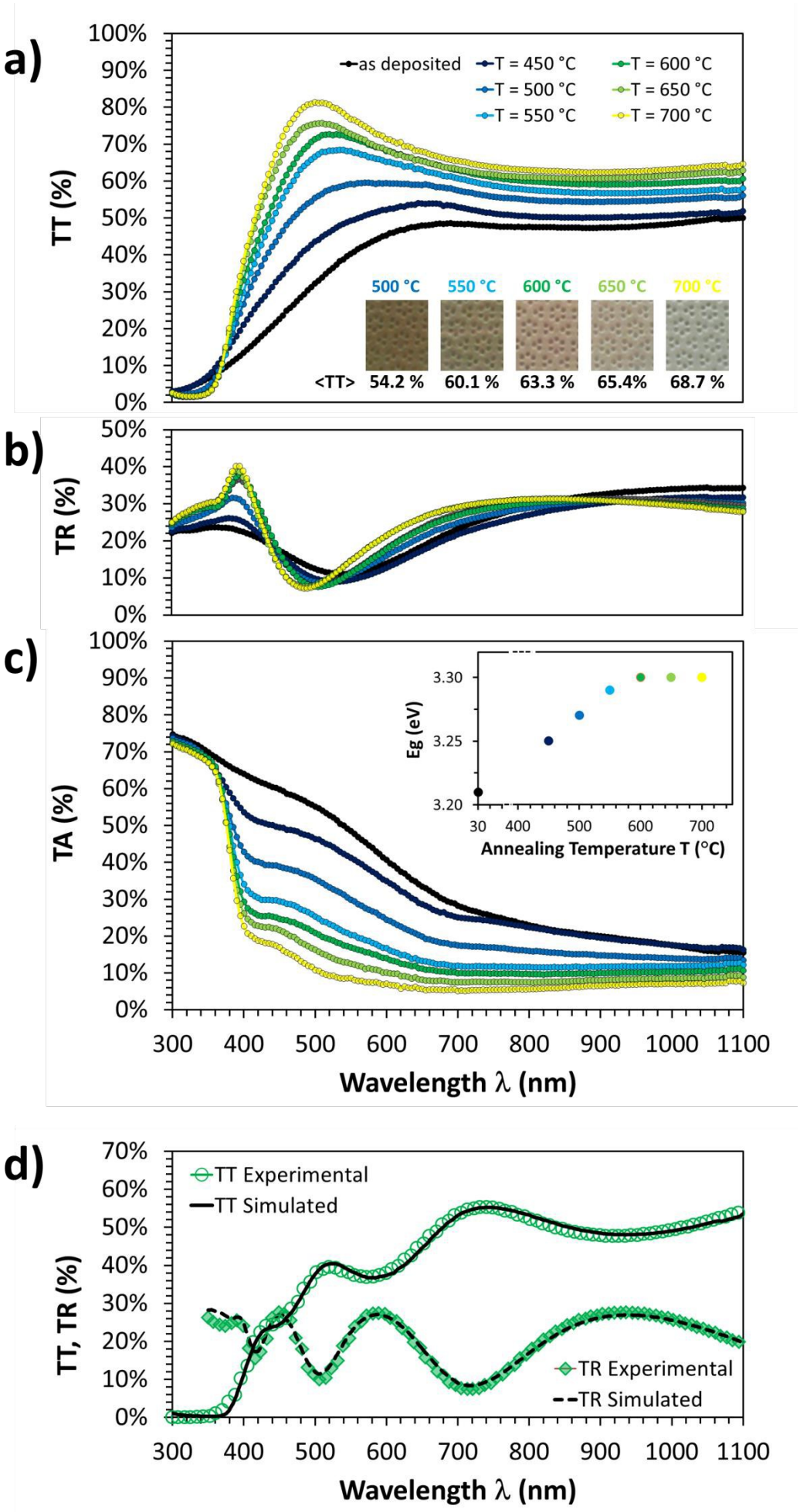

Figure 8

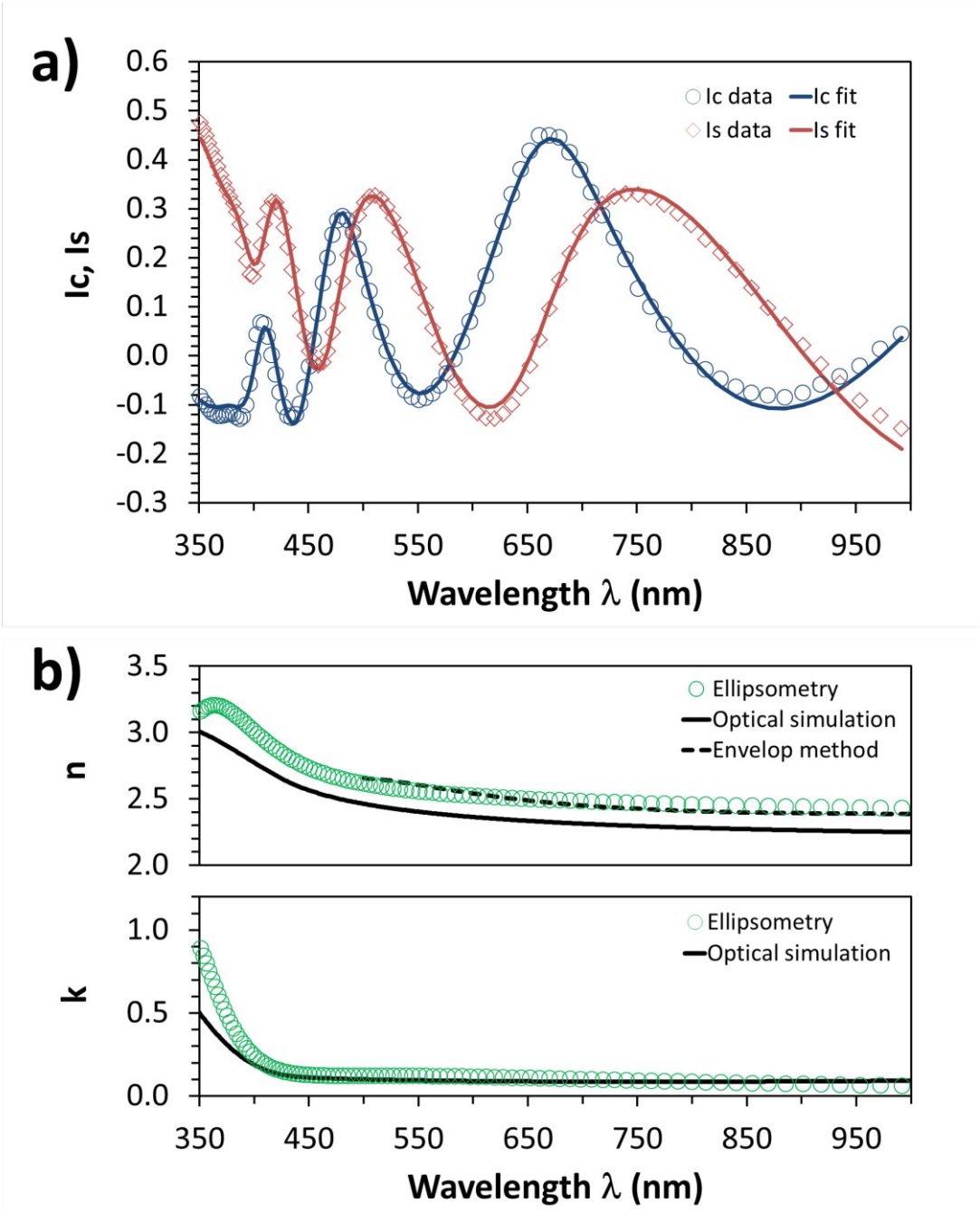

Graphical abstract